Efficient Techniques for Accurate Modeling and Simulation of Substrate Coupling in Mixed-Signal IC's

João Paulo Costa [*] Mike Chou [†] L. Miguel Silveira [*]

jpsc@algos.inesc.pt mtchou@rle-vlsi.mit.edu lms@algos.inesc.pt

[*] INESC/Cadence European Laboratories
Dept. of Electrical and Computer Engineering
Instituto Superior Técnico
Lisboa, 1000 Portugal

[†] Research Laboratory of Electronics
Dept. of Electrical Eng. and Computer Science
Massachusetts Institute of Technology
Cambridge, MA, 02139

Abstract

Industry trends aimed at integrating higher levels of circuit functionality have triggered a proliferation of mixed analog-digital systems. Magnified noise coupling through the common chip substrate has made the design and verification of such systems an increasingly difficult task. In this paper we present a fast eigendecomposition technique that accelerates operator application in BEM methods and avoids the dense-matrix storage while taking all of the substrate boundary effects into account explicitly. This technique can be used for accurate and efficient modeling of substrate coupling effects in mixed-signal integrated circuits.

1 Introduction

Industry trends aimed at integrating higher levels of circuit functionality resulting from an emphasis on compactness in consumer electronic products and a widespread growth and interest in wireless communications, have triggered a proliferation of mixed analog-digital systems. Single chip mixed-signal designs combining digital and analog blocks built over a common substrate, provide reduced levels of power dissipation, smaller package count, as well as smaller package interconnect parasitics. The design of such systems however, is becoming an increasingly difficult task owing to the various coupling problems that result from the combined requirements for high-speed digital and high-precision analog components. Noise coupling through the common chip substrate, caused by the nonideal isolation has been identified as a significant contributor to the coupling problem in mixed-signal designs [1, 2, 3, 4]. Fast switching logic components inject current into the substrate causing voltage fluctuation which can affect the operation of sensitive analog circuitry through the body-effect, since the transistor threshold is a strong function of substrate bias.

The most common way to deal with these problems is to resort to costly trial and error techniques. Clearly such a methodology, is not adequate in the face of rising fabrication costs and increasing demands for shorter design cycle times [4]. Several approaches have been presented in the past to attempt to quantify the effects of noise coupling through the substrate. Examples of such techniques include Finite Element (FEM) and Finite Diference (FD) numerical methods for computing all the currents and voltages in the substrate [1, 2, 5, 6, 7]. Unfortunately such methods are impractical for anything but simple problems, since the number of unknowns resulting from the discretization is too large because of volume-meshing of the entire substrate. Device simulators such as MEDICI and PISCES can also be used for this task. However they are in general too slow.

Boundary-Element methods (BEM) have been applied with some success to the problem of modeling substrate coupling. BEM methods are appealing for the solution of this type of problems because by requiring only the discretization of the relevant boundary features they dramatically reduce the size of the system to be solved. In [8] a Green's function for a two-layer substrate without backplane is used. In [9, 10] a distinct approach is taken in that point to point impedances are precomputed and later interpolated to find the admittance model. In both methods accuracy can be compromised due to the assumption of infinite lateral dimensions if some of the contacts are placed near the physical walls of the substrate. In [11] a Green's function is derived that takes into account the actual properties of the domain. Here a 2D DCT (Discrete Cosine Transform), implemented efficiently with an FFT algorithm, is performed thus avoiding repeated computation of the Green's function.

In general the computational effort involved in computing a model using BEM methods is considerable mostly because the matrices involved are dense. This fact has limited the usage of such methods to small to medium size

problems. In this paper we present a novel eigendecomposition method, used in a Krylov subspace solver, that eliminates dense-matrix storage and speeds up operator-vector application significantly. This method is used to speedup the computations necessary for computing substrate models in a BEM formulation and allows for the extraction of substrate models in problems containing several hundred surface unknowns. The resulting model can readily be incorporated into standard circuit simulators such as SPICE or SPECTRE to perform coupled circuit-substrate simulation.

In Section 2 we present some background on substrate coupling modeling and BEM methods. Then, in section 3 we present our algorithm based on a functional eigendecomposition of the substrate current to voltage operator and show how to use it to speed up substrate extraction. In section 4 the efficiency and storage requirements of the proposed method are discussed. In section 5 we include examples that illustrate the efficiency and accuracy of the techniques described. Finally, in section 6, we present some conclusions from our work.

2 Background

2.1 Problem Formulation

For typical mixed-signal circuits operating at frequencies below a few gigahertz, the substrate behaves resistively [3, 9]. Assuming this electrostatic approximation, the substrate can be modeled as a stratified medium composed of several homogeneous layers characterized by their conductivity, as shown in Figure 1. On the top of this stack of layers a number of ports or contacts are defined, which correspond to the areas where the designed circuit interacts with the substrate. Examples of these contacts include possible noise sources or receptors, such as contacts from substrate or wells to supply lines, drain/source/channel areas of transistors, etc. Figure 1 exemplifies the typical model assumed for the substrate and examples of contact areas or terminals. The contacts on the substrate top are usually assumed to be planar (bidimensional). The bottom of the substrate is either attached through some large contact to some fixed voltage (usually ground) or left floating.

In the electrostatic case the potential, ϕ satisfies Laplace's equation, $\nabla(\sigma\nabla\phi) = 0$, where σ is the substrate conductivity, assumed constant in each layer. Application of Green's theorem, assuming a modified Green's function $\boldsymbol{G}$ which accounts for the problem's boundary conditions gives the potential at some observation point (x, y) due to a unit current injected at some source point (x', y') as

$$\phi(x,y) = \int_S \boldsymbol{\rho}_s(x',y')\boldsymbol{G}(x,y,x',y')ds \qquad (1)$$

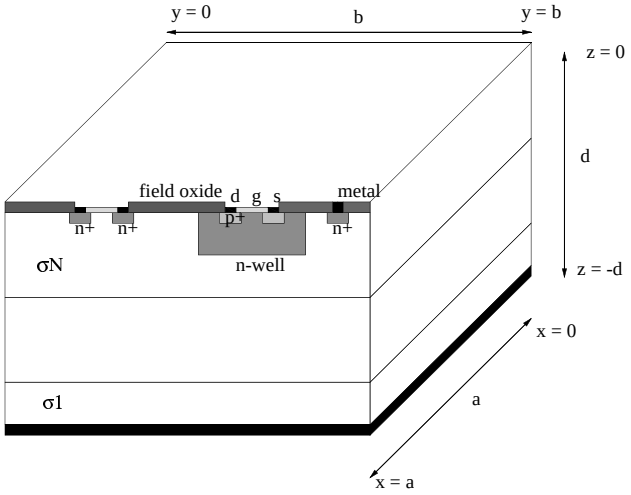

Figure 1: 3D model of the substrate as an homogeneous multilayered medium.

where $\boldsymbol{\rho}_s$ is the surface current density.

The usage of the medium's Green's function greatly simplifies the problem by implicitly taking into account the boundary conditions, making it unnecessary to discretize the boundaries. The substrate Green's function has been previously computed in analytical form and shown to be [3]

$$\boldsymbol{G} = \sum_{m,n=0}^{\infty} f_{mn}\cos(\alpha x)\cos(\alpha x')\cos(\xi y)\cos(\xi y') \qquad (2)$$

where $\alpha = m\pi/a$, $\xi = n\pi/b$, a and b are the substrate lateral dimensions and the f_{mn} can be computed with the help of recursion formulas. For the exact expressions and their derivation see [3] or [11].

2.2 Computing a Resistive Model

Once the Green's function is known, Eqn. (1) can be used to compute the potential at any point from a current distribution on the substrate contacts. Given a set of S contacts, we seek a model that relates the currents on those contacts, $\boldsymbol{I}_c$ to their voltage distribution $\boldsymbol{V}_c$,

$$\boldsymbol{I}_c = \boldsymbol{Y}_c\boldsymbol{V}_c. \qquad (3)$$

where $\boldsymbol{Y}_c$ is the admittance matrix of the system. The model given by Eqn. (3) is a simple resistive network where the contacts are the network nodes and entry (i, j) in $\boldsymbol{Y}_c$ represents the conductance between nodes i and j. Inclusion of such a model in a standard circuit simulator such as SPICE or SPECTRE is a trivial task.

Accuracy concerns make it necessary to discretize each of the contacts into a series of n panels ($n \gg S$). A set of

equations relating the currents and potentials on all panels can then be formulated

$$\boldsymbol{\phi}_p = \boldsymbol{Z}\boldsymbol{I}_p \tag{4}$$

where $\boldsymbol{Z} \in \mathbb{R}^{n\times n}$,

$$Z_{ij} = \frac{1}{S_i S_j}\int_{S_i}\int_{S_j} \boldsymbol{G}(x,y,x',y')da'da, \tag{5}$$

and S_i and S_j are the surface areas of panels i and j respectively.

Solving Eqn. (4) S times with an appropriate choice of contact potentials allows us to obtain the S columns of $\mathbf{Y}_c$ one at a time. The computational cost of such a task is dominated by the construction of $\boldsymbol{Z}$ and the solution of (4), S times. If Gaussian elimination (i.e. LU-factorization) is used to solve Eqn. (4), the computational cost will be $\mathcal{O}(n^3)$ which is overwhelming for typical values of n. Methods for speeding up the solution of this problem are however well known and have been applied to substrate extraction [9]. Iterative algorithms and namely Krylov-subspace algorithms can be used to speedup the solution of (4). An example of such a method is the Generalized Minimum Residual algorithm, GMRES [12]. GMRES solves the linear system by minimizing the norm of the residual $\boldsymbol{r}^k = \boldsymbol{\phi}_p - \boldsymbol{Z}\boldsymbol{I}_p^k$ at each iteration k, of the iterative process. The major cost of this algorithm is the computation of a matrix-vector product which is required at each iteration. Thus, if the number of iterations does not grow too rapidly and is kept small, the total cost of obtaining the substrate admittance model is $\mathcal{O}(S\ K_G\ n^2)$ where K_G is the average number of GMRES iterations per solution.

Using (2) directly to compute the elements of $\boldsymbol{Z}$ is computationally very expensive. Furthermore, since $\boldsymbol{Z}$ is dense, the storage requirements of such an algorithm are quite large making it impossible to handle large problems.

Therefore general methods have to be devised to avoid dense matrix storage and accelerate the computation of Eqn. (4) in order to be able to handle problems involving several hundreds of substrate contacts with high accuracy.

3 Sparsification via Eigendecomposition

In this section we describe the algorithm proposed for extracting a substrate model. Here the computation and thus the storage of $\boldsymbol{Z}$ is **unnecessary** as the iterative algorithm GMRES is used to solve Eqn. (4) but direct computation of the matrix-vector product, $\boldsymbol{Z}\boldsymbol{I}_p^k$ is **avoided**. This operation corresponds in essence to computing a set of average panel potentials given a substrate injected current distribution. This can readily be done by means of an eigenfunction decomposition of the linear operator that relates injected currents to panel potentials. As we shall see, this computation can be performed very efficiently by means of 2D DCT's.

3.1 Computation of the Operator Eigenpairs

The substrate top surface is first discretized in small rectangular panels, where small means that the current that flows across them can be considered uniformly distributed in each one. Considering the top of the substrate as a 2D surface, this discretization leads to an $M \times N$ set of panels (usually $M = N$). With this approximation the current distribution in the M by N panels can be represented by the following equation

$$\boldsymbol{q}(x,y) = \sum_{m=0}^{M-1}\sum_{n=0}^{N-1} q_{mn}\boldsymbol{\vartheta}\left(x-\alpha', y-\xi'\right) \tag{6}$$

where q_{mn} is the total current at panel (m,n), $\boldsymbol{\vartheta}(x,y)$ is a square-bump function that serves as an averaging function and is defined as

$$\boldsymbol{\vartheta}(x,y) = \begin{cases} \frac{MN}{ab} & \Leftarrow \quad -\frac{a}{2M} \le x \le \frac{a}{2M}, -\frac{b}{2N} \le y \le \frac{b}{2N} \\ 0 & \Leftarrow \quad elsewhere \end{cases}$$

and $\alpha' = (m+1/2)a/M$, $\xi' = (n+1/2)b/N$.

We now assume that the current distribution function $\boldsymbol{q}(x,y)$ can be represented (decomposed) by a sum of functions of the form

$$\boldsymbol{q}(x,y) = \sum_{i=0}^{\infty}\sum_{j=0}^{\infty} a_{ij}\ \boldsymbol{\varphi}_{ij}(x,y) \tag{7}$$

where $\boldsymbol{\varphi}_{ij}(x,y)$ are the functions and a_{ij} are the coefficients of the decomposition. If $\boldsymbol{\varphi}_{ij}(x,y)$ are the eigenfunctions of the linear operator $\boldsymbol{\mathcal{L}}$ which takes us from currents to potentials, then by definition, the potential can be written as

$$\boldsymbol{\Phi}(x,y) = \sum_{i=0}^{\infty}\sum_{j=0}^{\infty} \boldsymbol{\lambda}_{ij}\ a_{ij}\ \boldsymbol{\varphi}_{ij}(x,y) \tag{8}$$

where $\boldsymbol{\lambda}_{ij}$ are the eigenvalues of $\boldsymbol{\mathcal{L}}$. Therefore, if the eigenpairs (eigenfunctions and eigenvalues) of $\boldsymbol{\mathcal{L}}$ implied by Poisson's equation are known, and an eigendecomposition of the injected substrate currents can be obtained such as (7), then the potentials are trivially obtained from (8).

In order to compute the eigenpairs of $\boldsymbol{\mathcal{L}}$ we substitute (7) in Poisson's equation and note that the current distribution on the contacts is represented along the z axis as a delta function at $z = 0$. We obtain

$$\nabla^2\boldsymbol{\Phi}(x,y,z) = -\frac{\delta(z)\ \sum_{m=0}^{\infty}\sum_{n=0}^{\infty} a_{mn}\boldsymbol{\varphi}_{mn}(x,y)}{\sigma} \tag{9}$$

From the knowledge of the boundary conditions it is easy to show that this equation is satisfied if

$$\boldsymbol{\varphi}_{ij}(x,y) = \cos\left(\frac{i\pi x}{a}\right)\,\cos\left(\frac{j\pi y}{b}\right). \qquad (10)$$

and the eigenvalues $\boldsymbol{\lambda}_{mn}$ are the solution of

$$\frac{d^2\boldsymbol{\lambda}_{mn}(z)}{dz^2} - \gamma_{mn}^2\boldsymbol{\lambda}_{mn}(z) = -\frac{\delta(z)}{\sigma} \qquad (11)$$

evaluated at $z = 0$ ($\gamma_{mn} = \sqrt{(m\pi/a)^2 + (n\pi/b)^2}$). The solution of Eqn. (11) can be readily obtained to be, for $m, n \neq 0$,

$$\boldsymbol{\lambda}_{mn} = \frac{\beta_L \sinh(\gamma_{mn}d) + \Gamma_L \cosh(\gamma_{mn}d)}{\sigma_L\gamma_{mn}\left(\beta_L \cosh(\gamma_{mn}d) + \Gamma_L \sinh(\gamma_{mn}d)\right)} \qquad (12)$$

where L is the number of layers in the substrate profile with resistivities $\sigma_i, i = 1, \cdots, L$, and d its thickness. For $m = n = 0$, we get

$$\boldsymbol{\lambda}_{00} = \frac{\Gamma_L}{\sigma_L\beta_L}. \qquad (13)$$

The values of Γ_L and β_L can be computed in a recursive manner as in [11].

3.2 Eigendecomposition Representation for Panel Potentials

The expansion coefficients a_{ij} can be determined in the usual manner to be

$$a_{ij} = A_{ij}\int_0^a\int_0^b \boldsymbol{q}(x,y)\,\cos\left(\frac{i\pi x}{a}\right)\cos\left(\frac{j\pi y}{b}\right)dxdy \qquad (14)$$

Since $\boldsymbol{q}(x,y)$ is constant by rectangles as given by (6), replacing we obtain, after some algebra,

$$a_{ij} = A'_{ij}\sum_{m=0}^{M-1}\sum_{n=0}^{N-1} q_{mn}(x,y) \cos\left(\frac{(m+1/2)\pi i}{M}\right)\cos\left(\frac{(n+1/2)\pi j}{N}\right) \qquad (15)$$

with

$$A'_{ij} = \begin{cases} \frac{1}{ab} & \Leftarrow \quad i = 0, j = 0 \\ \frac{4N}{ab\pi j}\sin\left(\frac{\pi j}{2N}\right) & \Leftarrow \quad i = 0, j \neq 0 \\ \frac{4M}{ab\pi i}\sin\left(\frac{\pi i}{2M}\right) & \Leftarrow \quad i \neq 0, j = 0 \\ \frac{16MN}{ab\pi^2 ij}\sin\left(\frac{\pi i}{2M}\right)\sin\left(\frac{\pi j}{2N}\right) & \Leftarrow \quad i \neq 0, j \neq 0 \end{cases} \qquad (16)$$

From the knowledge of a_{ij} the potential distribution is readily computed from Eqn. (8). The average potential in each panel can then be obtained by taking the inner product between Eqn.(8) and the square-bump function supported over the given panel. The result of this operation is

$$\overline{\boldsymbol{\Phi}}_{pq} = \sum_{i=0}^{\infty}\sum_{j=0}^{\infty} C_{ij}\,\boldsymbol{\lambda}_{ij}\,a_{ij} \cos\left(\frac{(p+1/2)\pi i}{M}\right)\cos\left(\frac{(q+1/2)\pi j}{N}\right) \qquad (17)$$

with

$$C_{ij} = \begin{cases} 1 & \Leftarrow \quad i = 0, j = 0 \\ \frac{2N}{\pi j}\sin\left(\frac{\pi j}{2N}\right) & \Leftarrow \quad i = 0, j \neq 0 \\ \frac{2M}{\pi i}\sin\left(\frac{\pi i}{2M}\right) & \Leftarrow \quad i \neq 0, j = 0 \\ \frac{4MN}{\pi^2 ij}\sin\left(\frac{\pi i}{2M}\right)\sin\left(\frac{\pi j}{2N}\right) & \Leftarrow \quad i \neq 0, j \neq 0 \end{cases} \qquad (18)$$

Numerical evaluation of the average panel potentials, amounts to truncating Eqn. (17). The size of the summation is controlled by the number of coefficients a_{ij} available, and therefore by the number of cosine modes used in the eigendecomposition.

3.3 Efficient Computation of the Panel Potentials

Computing the average panel potentials from (17) given any arbitrary current distribution on the top of the substrate requires the computation of the a_{ij}. Inspection of Eqn. (15) reveals that, for $0 \leq i \leq M-1, 0 \leq j \leq N-1$, the coefficients a_{ij} are the result of a 2D type-2 DCT on the set q_{mn}. Such an operation can be efficiently performed by means of an FFT. Furthermore, after multiplication by the eigenvalues, computation of the average potentials from (17), assuming truncation of the summation, again amounts, up to a scaling factor, to the computation of an inverse 2D type-2 DCT on the set $C_{ij}\boldsymbol{\lambda}_{ij}a_{ij}$.

If necessary, the accuracy of the potential computation can be increased by further refining the substrate discretization. However this directly affects the number of panels in the system thus increasing the total computation time and storage. In our method, higher accuracy can be obtained, **without** refining the discretization, by increasing the size of the eigendecomposition, i.e., by employing more cosine modes. Apparently such an alternative would preclude usage of the efficient FFT algorithm for Eqn. (15) since there would now be more a_{ij} coefficients than panels (i.e. q_{mn} coefficients). However, by using the symmetry properties of the DCT, it can be shown that all $a_{ij}, i \geq M, j \geq N$ can be related to the first MN cosines modes (a_{ij}). This process is termed unfolding. Thus by simple computation of the DCT implied in (15), it is possible to obtain an arbitrary number of cosine mode coefficients without incurring in

any substantial extra cost. By a similar argument refolding of these coefficients can be performed to obtain the average panels potentials from (17). Specifically,

$$\overline{\boldsymbol{\Phi}}_{pq} = \sum_{i=0}^{M-1} \sum_{j=0}^{N-1} T_{ij}\, K_{ij} \cos\left(\frac{(p+1/2)\pi i}{M}\right) \cos\left(\frac{(q+1/2)\pi j}{N}\right) \quad (19)$$

where T_{ij} is the 2D DCT of q_{mn} as seen in (15) and

$$K_{ij} = \begin{cases} \frac{1}{ab}\boldsymbol{\lambda}_{00} & \Leftarrow \quad i=0, j=0 \\ \frac{8N^2}{ab\pi^2} \sin^2\left(\frac{\pi j}{2N}\right) \sum_{\hat{\jmath}} \frac{\boldsymbol{\lambda}_{o\hat{\jmath}}}{\hat{\jmath}^2} & \Leftarrow \quad i=0, j\neq 0 \\ \frac{8M^2}{ab\pi^2} \sin^2\left(\frac{\pi i}{2M}\right) \sum_{\hat{\imath}} \frac{\boldsymbol{\lambda}_{\hat{\imath}o}}{\hat{\imath}^2} & \Leftarrow \quad i\neq 0, j=0 \\ \frac{64M^2N^2}{ab\pi^4} \sin^2\left(\frac{\pi i}{2M}\right) \sin^2\left(\frac{\pi j}{2N}\right) \sum_{\hat{\imath}} \sum_{\hat{\jmath}} \frac{\boldsymbol{\lambda}_{\hat{\imath}\hat{\jmath}}}{\hat{\jmath}^2\hat{\imath}^2} & \Leftarrow \quad i\neq 0, j\neq 0 \end{cases} \quad (20)$$

$\hat{\imath} = i, \ldots, 2mM \pm i, m \in \mathbb{N}$ and similarly for $\hat{\jmath}$, where an appropriate number of terms is used.

4 Complexity Comparisons

In order to compare the memory usage and the computational cost (for similar accuracies) of the eigendecomposition algorithm proposed versus the Green's function based algorithm we will assume, without loss of generality, that the discretization of the substrate is such that $M = N$.

The memory requirements for the eigendecomposition method are $\mathcal{O}(k\, M^2)$ space to store the eigenvalues of the system, the DCT coefficients and the vectors necessary for the computation of the GMRES algorithm, and $\mathcal{O}(S^2)$ for the final admittance model (assuming S contacts are being used). The storage requirements for the Green's function based methods are $\mathcal{O}(P^2) + \mathcal{O}(n^2) + \mathcal{O}(S^2)$ where P is the size of the 2D grid used in the DCT and resulting from the panel discretization, n is the number of panels and S the number of contacts (usually $n \gg P$ and $n \gg S$). In [11] it is indicated that $\boldsymbol{Z}$ need not be explicitly computed, thus reducing the memory requirements. However this is done at the expense of increasing the computation cost by repeatedly assembling the $\boldsymbol{Z}_{ij}$ elements from the results of the 2D DCT sequence. The interesting case to consider is when the density of contacts is large, as is common in most designs where area is a major concern. In that case n can be a large percentage of P^2, which is the maximum number of contacts defined on a $P \times P$ grid. Typically M and P are of comparable magnitude for reasons of accuracy, even though as we saw, in the eigendecomposition method one can increase accuracy without increasing M. But even assuming that M and P are comparable, if $n \approx 20\% P^2$, a small density of contacts, the storage requirements of the Green's function methods are then $\mathcal{O}(P^2) + \mathcal{O}(n^2) = \mathcal{O}(P^2) + 0.04\,\mathcal{O}(P^4)$. For large enough P, the last term dominates the storage cost and the Green's function method requires substantially more space that the eigendecomposition method whose cost is always $\mathcal{O}(P^2)$, albeit with a large constant.

The computational cost of both methods can also be compared. For the Green's function method this cost is $\mathcal{O}(2P^2 \log(P)) + \mathcal{O}(n^2) + \mathcal{O}(S\ K_G\ n^2) = \mathcal{O}(2P^2 \log(P)) + \mathcal{O}(S\ K_G^{'}\ n^2)$, where the first term corresponds to the 2D type-1 DCT and the second term corresponds to stenciling the $\boldsymbol{Z}$ matrix and to the multiple system solutions if GMRES is used. It is easily seen that the second term always dominates the total cost. In the eigendecomposition method, the total cost is $\mathcal{O}(2M^2 \log(M)\ S\ K_E)$. Experience shows that K_E and K_G, the average number of GMRES iterations per contact in each method, are comparable. Thus the difference between the cost of the two methods rely on the comparison of $M^2 \log(M)$ to $n^2 = \alpha P^4$. As we saw previously, even for sparse designs in the number of contacts ($\alpha \approx 1\%$) $n^2 \gg M^2$, which implies that the eigendecomposition method is almost always much more efficient.

5 Experimental Results

In this section we present examples that show the accuracy and efficiency of the substrate coupling extraction algorithm presented in this paper. We will use as an example a layout from a simple mixed-signal circuit. Figure 2 shows the layout for an example problem with 52 contacts on a $128\mu m \times 128\mu m$ substrate.

Two experiments, using different substrate profiles were conducted on this example layout in order to test the versatility, accuracy and efficiency of the extraction algorithm. The profiles used were taken from [11] and are described in Figure 3. The high-resistivity substrate is used in various BiCMOS processes, while the low-resistivity substrate is used in CMOS due to their latch-up suppressing properties. For each of the substrate profiles, extraction was performed and a resistive model was obtained as described in Section 2.

Table 1 shows a selected set of relevant resistances computed using the Green's function based method and our eigendecomposition based method for the case of the low-resistivity profile. As seen from the table the accuracy of both methods is comparable. Similar accuracies were noted when the high-resistivity profile was employed.

In this example usage of a uniform discretization for the Green's function method would produce a problem

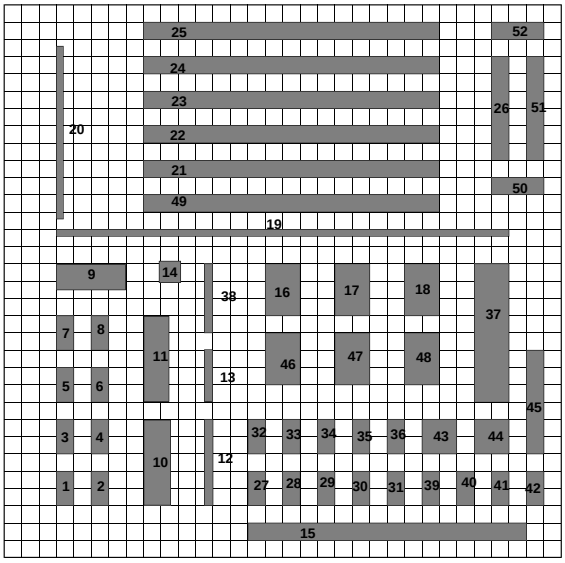

Figure 2: Example layout from a mixed-signal design.

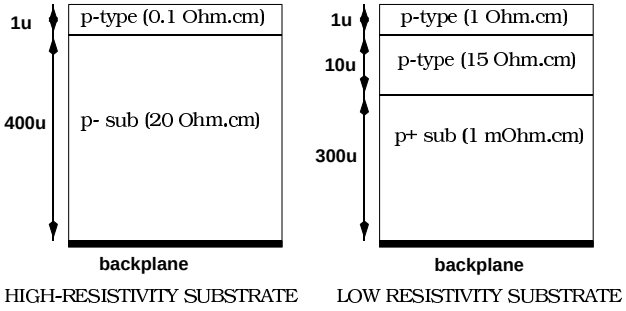

Figure 3: Substrate profiles used in example problem.

with too many panels and the computation time and memory requirements would be overwhelming. Therefore an efficient non-uniform discretization algorithm was implemented. The results in Table 2 show that the discretization using this algorithm produces a relatively small number of panels. This is a very important observation because it implies that an efficient discretization algorithm has to be developed if the Green's function method is to be applied for extraction. Tables 3 and 4 summarizes the relevant parameters obtained for the extraction applied to both the low and high-resistivity profile examples, respectively. In order to maintain similar accuracy between methods the minimal discretization used for each method was different. In particular a larger DCT was necessary for the Green's function based method. However, the cost of computing the DCT is not very relevant relative to the total cost, as seen in Tables 3 and 4. Also from Tables 3 and 4 one can see that the memory requirements for the eigendecomposition algorithm are much smaller. A factor of almost 6 was obtained in terms of memory savings.

Name	Nodes		Green's func	Eigendec.
	1	2	non-uni. dis.	unif. dis.
R0	1	BACK	2202.48	2203.45
R1	1	2	4689.54	4684.63
R400	9	21	5.55422e+06	7.46023e+06
R637	15	BACK	538.379	542.456
R678	16	19	5849.6	5711.85
R708	16	49	226888	245875
R712	17	BACK	1535.03	1539.48
R784	19	20	6626.83	6642.54
R839	20	42	7.82962e+07	7.83473e+07
R878	21	49	658.712	658.369
R1242	37	BACK	662.151	666.366
R1250	37	45	2632.51	2539.71
R1255	37	50	89315	94327.1
R1256	37	51	4.09985e+06	4.21027e+06

Table 1: Selected set of extracted resistances for the low-resistivity substrate. Node numbers refer to contacts and BACK refers to the grounded backplane.

Value	Green's func. non-unif. disc.	Eigendec. unif. disc.
# contacts	52	52
# panels	2647	17764
Avg. panels/contact	51	341
Size of DCT	512×512	256×256

Table 2: Summary of the relevant circuit parameters.

In terms of computational cost a factor of over 6 speedup was obtained for the low-resistivity substrate profile, and a speedup of almost 15 was recorded for the high-resistivity substrate, which leads to a harder numerical problem.

6 Conclusions

In this paper we reviewed some of the commonly used techniques for extracting and generating accurate models for substrate coupling. We presented a new eigendecomposition-based technique which when used in a Krylov subspace solver enables efficient extraction of a substrate coupling model in a BEM formulation. The resulting model can readily be incorporated into standard circuit simulators such as SPICE or SPECTRE to perform coupled circuit-substrate simulation. Examples that show the accuracy and efficiency of this extraction algorithm were

Value	Green's f. non-uni. dis.	Eigendec. unif. disc.
Memory usage	**142MB**	**23MB**
# GMRES iter.	1238	1868
Average per contact	23	35
Computation Times (seconds on an Ultra Sparc 1)		
discretization	0.06	0.54
Green's func. DCT	12.90	N/A
Total setup time	14241.5	12.5
Solve cost (GMRES)	16656.8	4111.4
Total extr. time	**30965.5**	**4994.9**

Table 3: Summary of the relevant parameters obtained for the extraction of the example problem for the low resistivity substrate profile.

Value	Green's f. non-uni. dis.	Eigendec. unif. disc.
Memory usage	**144.6MB**	**25.5MB**
# GMRES iter.	8030	2930
Average per contact	154	56
Computation Times (seconds on an Ultra Sparc 1)		
discretization	0.06	0.54
Green's func. DCT	10.33	N/A
Total setup time	14241.1	9.92
Solve cost (GMRES)	107278	6450.05
Total extr. time	**123630**	**8405.64**

Table 4: Summary of the relevant parameters obtained for the extraction of the example problem for the high resistivity substrate profile.

presented. A speedup of over 15 was obtained when comparing the new method with direct usage of the problem's Green's function for two substrate profiles. This result coupled with significant reductions in memory usage make the method presented very competitive for the solution of this problem.

Acknowledgments

This work was partially supported by the Defense Advanced Research Projects Agency, the National Science Foundation, the Portuguese JNICT programs PRAXIS XXI and FEDER under contracts 2/2.1/T.I.T/1661/95 and 2/2.1/T.I.T/1639/95 and grant BM-6853/95.

References

[1] David K. Su, Marc J. Loinaz, Shoichi Masui, and Bruce A. Wooley. Experimental results and modeling techniques for substrate noise in mixed-signal integrated circuits. *IEEE Journal of Solid-State Circuits*, 28(4):420–430, April 1993.

[2] T. A. Johnson, R.W. Knepper, V. Marcellu, and W. Wang. Chip substrate resistance modeling technique for integrated circuit design. *IEEE Transactions on Computer-Aided Design of Integrated Circuits*, CAD-3(2):126–134, 1984.

[3] Ranjit Gharpurey. *Modeling and Analysis of Substrate Coupling in Integrated Circuits*. PhD thesis, Department of Electrical Engineering and Computer Science, University of California at Berkeley, Berkeley, CA, June 1995.

[4] Bram Nauta and Gian Hoogzaad. How to deal with substrate noise in analog cmos circuits. In *European Conference on Circuit Theory and Design*, pages Late 12:1–6, Budapest, Hungary, September 1997.

[5] Sujoy Mitra, R. A. Rutenbar, L. R. Carley, and D. J. Allstot. A methodology for rapid estimation of substrate-coupled switching noise. In *IEEE 1995 Custom Integrated Circuits Conference*, pages 129–132, 1995.

[6] Balsha Stanisic, Nishath K. Verghese, Rob A. Rutenbar, L. Richard Carley, and David J. Allstot. Addressing substrate coupling in mixed-mode ic's: Simulation and power distribution systems. *IEEE Journal of Solid-State Circuits*, 29(3):226–237, March 1994.

[7] Ivan L. Wemple and Andrew T. Yang. Mixed-signal switching noise analysis using voronoi-tesselation substrate macromodels. In 32^{nd} *ACM/IEEE Design Automation Conference*, pages 439–444, San Francisco, CA, June 1995.

[8] T. Smedes, N. P. van der Meijs, and A. J. van Genderen. Extraction of circuit models for substrate cross-talk. In *International Conference on Computer Aided-Design*, San Jose, CA, November 1995.

[9] Nishath K. Verghese, David J. Allstot, and Mark A. Wolfe. Verification techniques for substrate coupling and their application to mixed-signal ic design. *IEEE Journal of Solid-State Circuits*, 31(3):354–365, March 1996.

[10] Nishath Verghese. *Extraction and Simulation Techniques for Substrate-Coupled Noise in Mixed-Signal Integrated Circuits*. PhD thesis, Department of Electrical and Computer Engineering, Carnegie Mellon University, Pittsburgh, PA, August 1995.

[11] Ranjit Gharpurey and Robert G. Meyer. Modeling and analysis of substrate coupling in integrated circuits. *IEEE Journal of Solid-State Circuits*, 31(3):344–353, March 1996.

[12] Y. Saad and M. H. Schultz. GMRES: A generalized minimal residual algorithm for solving nonsymmetric linear systems. *SIAM Journal on Scientific and Statistical Computing*, 7:856–869, July 1986.